Effects of Bearing Surfaces on Lap Joint Energy Dissipation

Harold R. Kess[1], Nathan J. Rosnow[2], Brian C. Sidle[3]

[1]Department of Mechanical Engineering, Purdue University, West Lafayette, IN. 47907
[2]Department of Engineering Physics, University of Wisconsin-Madison, Madison, Wisconsin. 53706
[3]Department of Mechanical Engineering, University of Houston, Houston, Texas. 77204

ABSTRACT

Energy is dissipated in mechanical systems in several forms. The major contributor to damping in bolted lap joints is friction, and the level of damping is a function of stress distribution in the bearing surfaces. This study examines the effects of bearing surface configuration on lap joint energy dissipation. The examination is carried out through the analysis of experimental results in a nonlinear framework. Then finite element models are constructed in a nonlinear framework to simulate the results. The experimental data were analyzed using piecewise linear log decrement. Phenomenological and non-phenomenological mathematical models were used to simulate joint behavior. Numerical results of experiments and analyses are presented.

NOMENCLATURE

$[\boldsymbol{m}]$	mass matrix
$[\boldsymbol{c}]$	linear viscous damping matrix
$[\boldsymbol{k}]$	stiffness matrix
$\{\boldsymbol{x}\}$	response vector
$R(\varphi_1\xi,\varphi_1\dot{\xi})$	nonlinear friction force
$\sigma,\ F_c$	Dahl model parameters
$\sigma_0,\sigma_1,\alpha_0,\alpha_1,\alpha_2,v_0,v_d$	LuGre model parameters

INTRODUCTION

All mechanical systems exhibit damping characteristics. These characteristics can be the result of (1) energy dissipation within the material of the system, (2) radiation of energy into the surrounding medium (air, water, soil, the system itself, and other mechanical devices), (3) the frictional interaction between elements of a structure and consequent energy dissipation at the microscopic or macroscopic level due to roughness of the material (asperities), and (4) components such as dampers that are designed to remove energy from a system in a controlled manner. (Thomson, 1988)

Friction is present in mechanical systems where relative motion occurs at one or more physical interfaces between surfaces in contact. The presence of friction in mechanical systems can be desirable or detrimental, depending on the type of system under consideration. Friction is a nonlinear phenomenon and, therefore, can cause tracking errors, limit cycles, steady-state errors, and undesired stick-slip motion. As well, friction leads to energy dissipation, which results in diminished motion, and this can influence the reliability of the system. According to Olsson, et al. (1998) many different mechanisms influence the effects of friction such as contact geometry and topology, properties of the surface materials of the bodies, and the presence of lubrication.

Both macro- and micro-slip result in energy dissipation in mechanical systems and are frequently the dominant damping mechanisms in structures. Macro-slip occurs in a lap joint when there is relative motion over the contact area between two surfaces, and does not occur until the two surfaces are pulled in opposite direction by a sufficiently large force. Micro-slip occurs in a lap joint when relative motion occurs over any portion (either large or very small) of the contact area between adjacent surfaces.

Bolted lap joints are used in a variety of applications ranging from bridges to aircraft structures because they are inexpensive and easy to fabricate. This investigation examines the effects of stress distribution on lap joint energy dissipation. To do so, washers are used to alter the stress distribution at the bearing surfaces. Relationships involving energy dissipation are determined by performing three experiments, in an attempt to validate two hypotheses. The hypotheses are: (1) That the local equivalent linear damping (and therefore energy dissipation) is a function of the amplitude at low levels of motion. (We anticipate that at low levels of motion energy dissipation tends to increase with amplitude of motion.), (2) The equivalent linear damping (and, therefore, energy dissipation) in a lap joint is a function of the bearing area over which micro-slip can potentially occur. (We anticipate that for small bearing areas, energy dissipation tends to increase as a function of area.)

The specimen that was used in the experiments consists of two beams connected by two plates bolted together. A schematic of the specimen is shown in Figure 1. The beam and plate interfaces create the desired lap joints to be analyzed and tested.

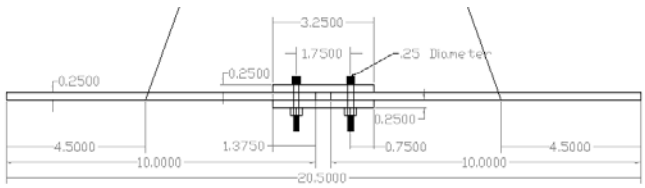

Figure 1: Schematic of Jointed Beam Specimen

Each experiment was performed according to the procedure outlined in a later section. An impact hammer was used to excite the structure, and the dynamic response was measured. The excited beam exhibits response amplitudes characterized by monotonic decay, and the first mode shape resembles the schematic shown in Figure 2. In addition the locations where washers were added in some of the experiments are shown by capital letters.

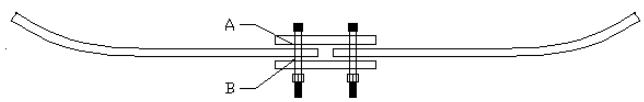

Figure 2: First Excited Modal Shape of the Beam

In the first experiment the friction effects on dynamic response corresponding to the absence of any washers at A and B were investigated. This configuration established the greatest possible bearing area where micro-slip can potentially occur. The second experiment involved placing large diameter washers at A and B in the lap joints. This configuration diminishes the bearing area where micro-slip can occur. The third experiment involved placing small diameter washers at A and B. This final configuration further diminishes the bearing area where micro-slip can occur.

In order to predict the characteristic behavior in frictional joints an accurate frictional model is required. There have been numerous models proposed ranging from static to dynamic models based on phenomenological and non-phenomenological observations of sliding friction. Most of the existing models use classical friction. These are acceptable for high velocity applications, but for low velocity applications these models are not sufficient. In this paper we consider two friction models for the mathematical simulation of the experimental results.

The first model considered to represent friction in the lap joints is the Dahl model (Dahl, 1976). The Dahl model, which was developed to simulate control systems with friction, was constructed with reference to the stress-strain curve in classical mechanics. The friction force in this model is only a function of the displacement and the sign of the velocity. Therefore, the model is considered to be rate independent and as a result does not capture the Stribeck effect (Gaul and Nitsche), a rate dependent phenomenon. The model does not account for stiction.

The second friction model considered to describe the friction in the bolted lap joints is the LuGre model (Olsson, et al. 1998). The LuGre model (Lund-Grenoble) combines the effects of the Dahl model and the bristle model (Haessing and Friedland, 1991) and has more parameters than the Dahl model. Therefore, it should have the potential to model joint friction more accurately. This model accounts for both the Stribeck effect and stiction.

In the following sections we (1) quantitatively describe the principles associated with the energy dissipation in the micro-slip domain, (2) describe the experimental configuration and the testing and data analysis procedures used for the experiments, (3) describe the two damping models and an approximate finite element model created to simulate the experimental findings, and (4) present the experimental and analytical results. Finally, conclusions and recommendations for future investigations are offered.

PRINCIPLES OF ENERGY DISSIPATION IN MICRO-SLIP

Structures with lap joints display higher damping than analogous structures with monolithic construction in place of lap joints because friction occurs in lap joints. This friction can be modeled in many different ways; however, for the purpose of this discussion, consider Coulomb friction. Coulomb friction can be explained using the simple model in Figure 3.

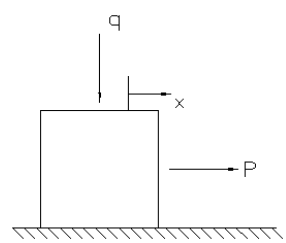

Figure 3: Simple Coulomb Friction Model

Friction occurs at the interface between the block and the rigid surface. P is an external lateral force, and q the normal force acting on a rigid block. No displacement occurs, in Coulomb friction, when $P < q\mu_s$, where μ_s is the coefficient of static friction. However, once P exceeds the limiting Coulomb static friction force, $q\mu_s$, sliding commences and the friction restoring force becomes $P = q\mu_d$, where μ_d is the coefficient of dynamic friction. Typically, $\mu_s > \mu_d$. Therefore, Coulomb friction prevents motion form occurring until an adequate tangential force is realized and then opposes that force once motion occurs. When sliding occurs, energy is dissipated in the system. The phenomenon described here is macro-friction because motion occurs over the entire contact surface between the rigid block and the rigid surface that supports it. Before sliding commences no energy is dissipated. After sliding starts, energy is dissipated because of friction. The amount of energy dissipated is proportional to the normal force.

In the case of lap joints, high normal loads applied by connecting bolts limit relative motions between components. The schematic in Figure 4a shows a lap joint in the beam tested in this investigation. As the beam vibrates, it bends. The beam bending causes generation of shear stresses on

the bearing surfaces of the lap joints. When the limiting friction force is high, no slippage occurs immediately under the bolt. However, away from the bolt, the normal stresses due to clamping are smaller, and in these regions, small slippage can occur. This slippage that occurs over a fraction of the region of contact results in micro-slip.

An easy way to visualize the micro-slip-related damping in the lap joint is to consider a simple, spatially discretized system in Figure 4b that models the lap joint. Each beam connecting into the lap joint is divided into rigid elements and the elements are connected with springs. The springs have constants reflecting the stiffness of the beam material. The lap joint clamping load is applied to the blocks in the discretized model. The equal and opposite clamping forces are great in the center, where the bolt is modeled, and smaller away from that point.

The phenomenon of micro-slip in the joint can be seen readily. When the clamping force, *q*, associated with the bolt is large, slippage between elements A and B may never occur. Yet the clamping force away from the bolt diminishes. Slippage occurs at the interface between elements C and D when the forces are large enough to overcome both the sliding friction between the elements and the stretching of the connecting springs. This slippage may occur quite readily away from the lap joint bolt where the clamping force is low. This slippage results in energy dissipation due to micro-slip.

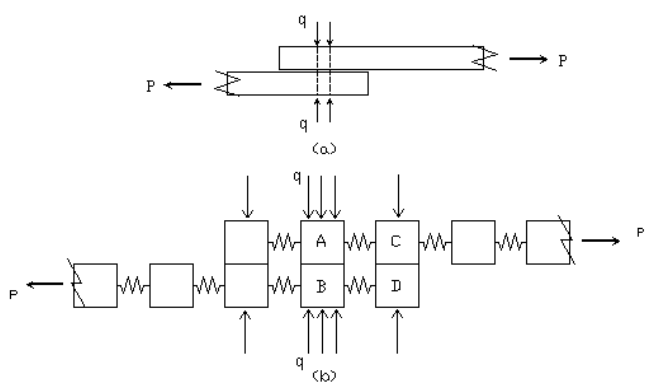

Figure 4: Modeling and Discretization of Lap Joint

EXPERIMENTAL CONFIGURATION AND PROCEDURES

The basic test structure used in the experiments of this investigation is shown schematically in Figure 1. The structure consists of four 0.25 inch thick and 1 inch wide steel beams. The two main beams are ten inches in length and are sandwiched between two 3.25 inch beams. Two 0.25 inch steel bolts that are tightened to 85 in-lbs establish the joint. This configuration leaves a 0.3125 inch space between the bolted ten inch beams.

To test the hypotheses specified in the introduction, three variations on the basic testing configuration of the lap joint were devised. The interior surfaces of interest in the joint were labeled in Figure 2. In the three experiments (a) no washer, (b) large diameter washers, and (c) small diameter washers were placed at these bearing surfaces. The large and small washers are 0.75 and 0.5 inches, respectively, in outer diameter. Experiments were performed in the three configurations.

In order to assemble the lap joint as precisely as possible for each configuration, a standard assembly procedure was developed. First, all beam components are laid out in the correct configuration for assembly standing on their edges. The bolts are run through the lined up holes, placing the appropriate washers in the correct bearing surfaces. Then the joint is held in tension from the ends of the long beams while the bolts are torqued to 85 in-lbs. To create the free-free boundary conditions for the experiment, the lap joint is then hung from a tripod using rubber tubing (see photo in Figure 5). The tubing suspends the lap joint at points 4.5 inches away from the ends of the long beams, where first mode nodes were experimentally located.

Figure 5: Shows the experimental set up including beam, tripod and rubber tubing

The beam was instrumented with an Endevco Isotron® 2250A-10 accelerometer fixed with wax to the beam, 0.5 inches outside the joint (see photo in Figure 6). The accelerometer sensitivity and range were 10.01 mV/g and +/- 500 g respectively. A PCB 086C03 impact hammer with a rubber tip was used to excite the beam at the desired frequencies. The hammer impacted the beam along the central axis, 0.5 inch from the end opposite the accelerometer. The force transducer on the impact hammer has a range of 0-500 lbf. and sensitivity of 10 mV/lbf.

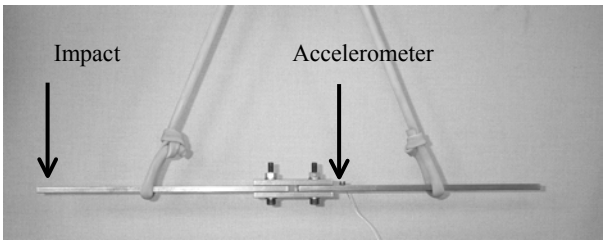

Figure 6: Shows accelerometer placement and impact location on the beam

All force and acceleration data were collected through the Dactron four-channel Photon dynamic system analysis data acquisition system using Dactron's RT Pro Dynamic Signal Analysis software on a desktop computer running Microsoft Windows 2000. Data were recorded for 3.1996 s at a rate of 2560 samples/s. The data acquisition system is triggered when the hammer force surpasses 1 lbf. A 25 sample buffer is included at the beginning of each run. Although ten runs were averaged to estimate the beam frequency response functions, each time response was saved individually. The time domain files of both the hammer and the accelerometer were exported as ASCII text files and analyzed in MATLAB.

Denote the measured acceleration response $x_j, j = 0,1,\ldots,n-1$. The objective of the data analysis is to estimate the local linear damping factor in the first mode of response as a function of response velocity amplitude. This is accomplished as follows. The frequency response function of the structure at a point is estimated using multiple realizations of the measured excitation and response. The frequency response function is then used to infer the structural modal frequencies, and all the measured response signals used in the investigation are band-pass filtered to obtain the component of response associated with the first structural mode. Denote the filtered, first mode response $x_j^{(f)}, j = 0,1,\ldots,n-1$.

The first modal frequency is approximately 125 Hertz. The band pass filter has a tenth order Butterworth filter with pass band [100,150] Hertz. Next each filtered first mode response is Hilbert transformed to establish the envelope of filtered response. Let $\hat{x}_j^{(f)}, j = 0,1,\ldots,n-1$ denote the discrete Hilbert transform of the filtered, first mode response data. Then the envelope of the first mode response data is:

$$e_j = \sqrt{[x_j^{(f)}]^2 + [\hat{x}_j^{(f)}]^2}, \quad j = 0,1,\ldots,n-1 \tag{1}$$

These envelope data are to be used to estimate the equivalent damping factor of the first mode of response in the experimental system. Log decrement is the method to be used to establish the estimate.

The log decrement approach is implemented in a local linear construct to approximate energy dissipation. The impulse response function of the first mode of a linear multi-degree-of-freedom system has the form:

$$x(t) = e^{-\zeta_1\omega_1 t}(c_1 \sin\omega_{d1}t + c_2 \cos\omega_{d1}t), \quad t \geq 0 \tag{2}$$

where c_1 and c_2 are constants relating to the amplitude, ζ_1 is the damping factor of the first mode, ω_1 is the first modal frequency, and ω_{d1} is the first damped modal frequency. This form can be digitized by evaluating the equation at $t = j\Delta t, j = 0,1,\ldots,n-1$, where Δt is the time increment of the recorded data points. The theoretical envelope of the impulse response is:

$$e_j = ce^{-\zeta_1\omega_1 j\Delta t} \tag{3}$$

Equate the right side expressions in Eq. (1) and (3), take the logarithm on both sides of the equation, and estimate the damping factor ζ_1 by using a least squares computation involving time indices that cover a small range of values. Use the values of the envelope, e_j with the same time indices, to evaluate the average envelope amplitude. The results are an estimate of local equivalent first mode damping factor and its associated amplitude.

This procedure is applied to data sets from experimental and numerical results in a section to follow, and graphic results are presented below.

MATHEMATICAL MODEL

The limited scope of this investigation precluded the specification of a mathematical model in the predictive framework. Because it is preferable not to require experiments to obtain an accurate simulation for structures with joints, the development of a mathematical model is still of great interest. In view of this we desire to create a finite element model of the beam shown in Figure 1 using some standard friction models from the literature. In particular we used the Dahl and LuGre models to simulate the dissipation of energy in the lap joint. We start be giving a brief overview of each model.

The Dahl model was initially established to simulate control systems with friction and for adaptive friction compensation, but it has also been shown to approximate the solid friction between metal surfaces (Olsen, et al. 1998). Dahl's model allows for the simulation of the dissipative frictional force, and in this investigation was used to approximate the energy dissipation at the bearing surfaces of a lap joint. The governing equations for the Dahl model are:

$$\frac{dz}{dt} = v - \frac{\sigma\,|\,v\,|}{F_c} z \tag{4a}$$

$$F = \sigma z \tag{4b}$$

where F is the restoring friction force, z is an auxiliary variable of the friction model that is related to the bristle deformation in the bristle model. (Haessing and Friedland, 1991), σ is the rest stiffness and is related to the bristle stiffness, F_c is the limiting Coulomb friction, and v is the relative velocity between the contact surfaces where friction occurs.

According to Eq. 4 the friction force is only a function of the displacement and the sign of the velocity. Therefore, the Dahl model is a rate independent model and does not capture the Stribeck effect, nor does it account for stiction. In addition, this model characterizes the energy dissipation that occurs as a result of hysteretic work loss in the lap joint as the beam flexes in bending. An example of the variation in the friction force as a function of the relative displacement between surfaces is shown in Figure 7. Values of $\sigma = (2\pi)^2$ and $F_c = 38$ were used to generate the plotted results.

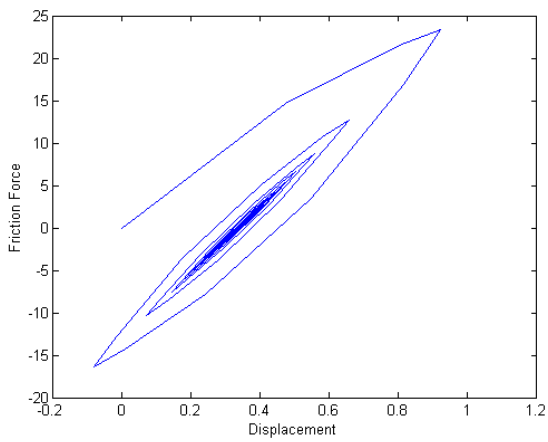

Figure 7: Friction force versus displacement for Dahl model

The LuGre model is a generalization of the Dahl model, and incorporates the bristle interpretation established in the bristle model. The bristles represent the asperities present at the microscopic level of the surfaces. In this investigation a standard parameterization of the LuGre model was used. This special case accounts for linear viscous damping and nonlinear friction interface. The model is given by:

$$\frac{dz}{dt} = v - \frac{\sigma_0 |v|}{g(v)} z \tag{5a}$$

$$F = \sigma_0 z + \sigma_1 \dot{z} + \alpha_2 v \tag{5b}$$

$$g(v) = \alpha_0 + \alpha_1 e^{-(v/v_0)^2} \tag{5c}$$

$$\sigma_1(v) = \sigma_1 e^{-(v/v_d)^2} \tag{5d}$$

where F is the frictional force, v is the relative sliding velocity at the friction interfaces, σ_0 is the bristle stiffness, σ_1 is the nonlinear damping coefficient, α_0 is the Coulomb friction force, $\alpha_0 + \alpha_1$ is the stiction force, and α_2 is the linear viscous friction coefficient.

The LuGre model, unlike the Dahl model, is a rate dependent friction model and, therefore, accounts for the Stribeck effect and stiction phenomenon. In addition, as a result of being rate dependent this model also captures the varying break-away force and frictional lag phenomenon. It should be noted that the Dahl model can be obtained from the LuGre model by setting $\sigma_1 = \alpha_2 = 0$ and $g(v) = F_c/\sigma_0$. The LuGre model also exhibits the same hysteretic energy dissipation characteristics that were shown for the Dahl model in Figure 7. The following figure shows the analogous friction force versus displacement for the LuGre model when the parameters were given values of $\sigma_0 = (2\pi)^2$, $\sigma_1 = .008(\pi)$, $\alpha_0 = 38$, $\alpha_1 = .5\alpha_0$, $\alpha_2 = \sigma_1$, and $v_d = v_0 = 1$.

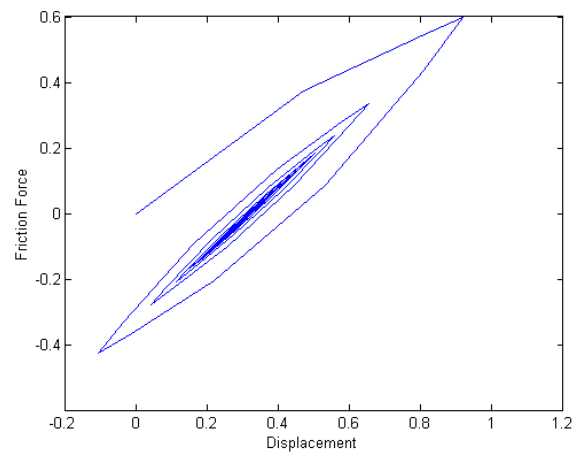

Figure 8: Friction force versus displacement for LuGre model

Because the objective of this part of the investigation is merely to explore the plausibility of the friction models described above for the simulation of lap joint friction in the structure shown in Figure 1, it is sufficient to simulate the system behavior using an approximate nonlinear finite element analysis. To construct this analysis the following steps were taken. First the partial differential equation governing the motion of the system was approximated by the matrix system of ordinary differential equations:

$$\boldsymbol{m}\ddot{\boldsymbol{x}} + \boldsymbol{c}\dot{\boldsymbol{x}} + \boldsymbol{k}\boldsymbol{x} + \boldsymbol{R}(\boldsymbol{x}, \dot{\boldsymbol{x}}) = \boldsymbol{0} \tag{6}$$

where $\boldsymbol{x}$ denoted the vector of displacement at structural degrees of freedom, dots denote differentiation with respect to time, $\boldsymbol{m}$ is the mass matrix, $\boldsymbol{c}$ is the linear viscous damping matrix, $\boldsymbol{k}$ is the stiffness matrix, and $\boldsymbol{R}(\boldsymbol{x}, \dot{\boldsymbol{x}})$ is the nonlinear restoring force vector. We can rearrange the governing equation by moving the nonlinear term to the right hand side:

$$\boldsymbol{m}\ddot{\boldsymbol{x}} + \boldsymbol{c}\dot{\boldsymbol{x}} + \boldsymbol{k}\boldsymbol{x} = -\boldsymbol{R}(\boldsymbol{x}, \dot{\boldsymbol{x}}) \tag{7}$$

Next a modal analysis using the mass and stiffness matrices was performed. This yields a sequence of modal frequencies ω_k, $k = 1, \ldots, M$, and mode shapes φ_k, $k = 1, \ldots, M$ for the system. Then mass normalize the mode shapes so that $\varphi_k^T m \varphi_k = 1$. Because the experiments to be discussed later filter the motions so that only the first oscillatory mode is present, the current model must be required to respond only in the first mode. This is done by writing:

$$x = \varphi_1 \xi \tag{8}$$

where φ_1 is the first mode shape, and ξ is the coordinate of motion in the first mode. Use this in Eq. (7) to obtain:

$$\ddot{\xi} + 2\varsigma\omega\dot{\xi} + \omega^2\xi = -\varphi_1^T R(\varphi_1\xi, \varphi_1\dot{\xi}) \qquad (9)$$

This is the equation of motion for a nonlinear single-degree of freedom system. In this investigation this equation was solved using the Runge-Kutta method. The restoring force $R(\varphi_1\xi, \varphi_1\dot{\xi})$ is negative the friction force F specified in the models above. Note that the auxiliary variable, z, in either friction model must be included in the state vector during numerical solution of Eq. (9). Some examples of the numerical solutions of Eq. (9) using both friction models are presented in the following section.

EXPERIMENTAL AND ANALYTICAL RESULTS

The experiments described in a previous section were performed and system excitations and responses were measured. One measured acceleration response time history is shown in Figure 9. The figure shows the filtered acceleration response for the no washer-configured beam with filter pass band [100, 150] Hz. The time history also shows the envelope formed as described in Eq. (1). The envelopes were analyzed as specified in the Analysis of Experimental Data Section. Local linear estimates of damping factors were computed for all three-beam configurations and are shown in Figures 10, 11, and 12. The figures depict local linear estimates of damping factors as a function of velocity amplitudes. The first presents this information for the no washer beam, the second for the large washer beam, and the third for the small washer beam. Each figure presents the results of 10 tests. Each decaying amplitude envelope was divided into several overlapping segments. Each segment corresponded to about 10 cycles of motion. This sampling explains the number of local linear damping factor estimates shown in the figures.

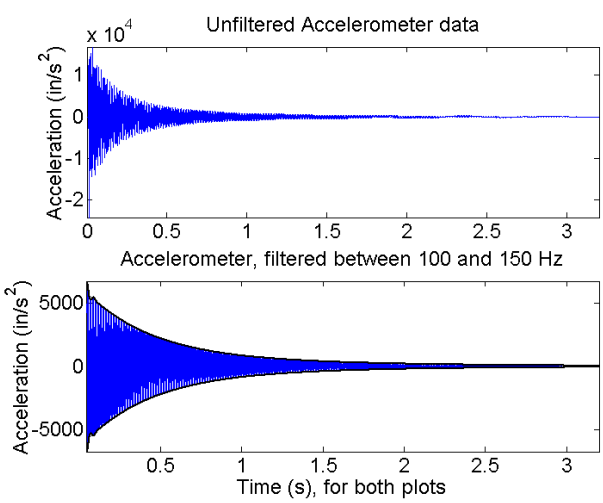

Figure 9: Unfiltered and Filtered Time history of the no washer-configured beam

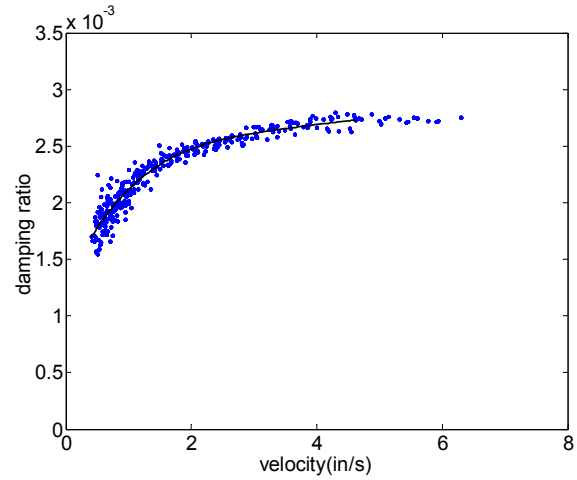

Figure 10: Estimates of local linear damping factor versus velocity amplitude for the no washer beam.

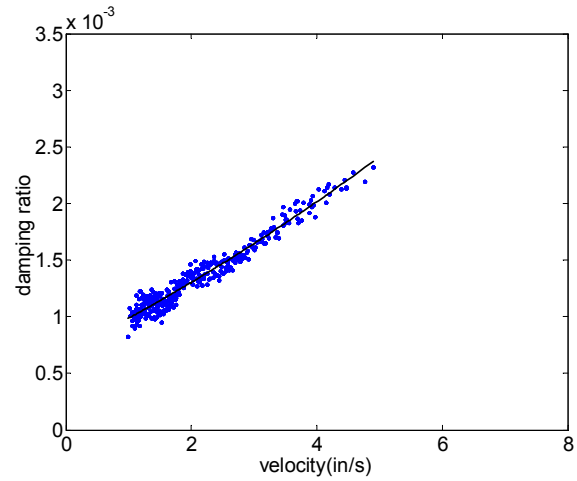

Figure 11: Estimates of local linear damping factor versus velocity amplitude for the large washer beam.

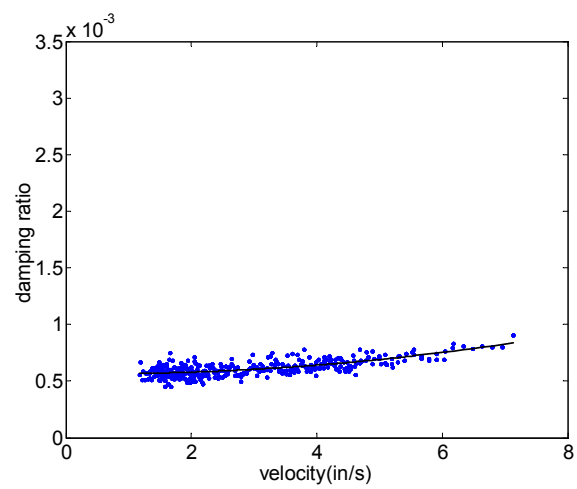

Figure 12: Estimates of local linear damping factor versus velocity amplitude for the small washer beam.

These results make it clear that damping of a beam with a lap joint is a function of the velocity amplitude. As shown previously in the discretized representation of the beam, the motion that occurs in the lap joint causes a friction restoring force that opposes that motion, and thus acts to stop the vibrations. The behavior of the no-washer system indicates diminishing slope of the damping factors with increasing velocity amplitude. This implies an upper bound on damping for the lap joint beam.

Damping levels in the three beam configurations tested differ as shown in Figures 10, 11, and 12. These differences correspond to differences in lap joint bearing area. The area over which micro-slip can potentially occur are: 1.36 in^2 for the no-washer configuration, and 0.66 in^2 and 0.17 in^2 for the larger and smaller diameter washer configurations respectively. These areas are the total contact area minus the bolt head area. Note that micro-slip can occur on both surfaces of the washers, and this part is accounted for in the area computation.

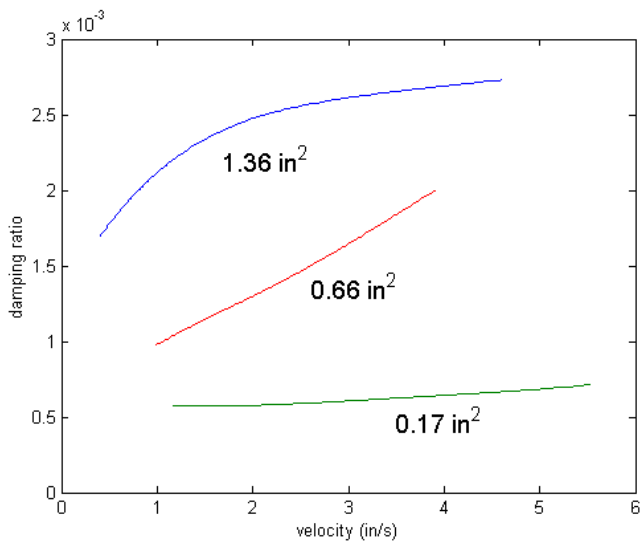

Figure 13: Shows the damping ratios versus velocity amplitudes against the bearing areas in the joints

Figure 13 shows polynomial fits to the data in Figures 10, 11, and 12. The curves indicate that the damping in the lap joint is dependent on the size of the frictional area. For the case of the small washer, the effective area is so small that damping force is high and, therefore, little energy dissipation occurs. Damping is almost constant with amplitude as in the linear viscous case. On the other hand the no-washer joint, with a large effective area, exhibits a very nonlinear damping behavior.

The nonlinear finite element model described in the mathematical model section was used in conjunction with the Dahl and LuGre models to determine their plausibility in simulating the experimental results. Only the case where there are no washers present between the frictional interfaces were considered in the comparison of the experimental results to the mathematical models.

The Dahl model has two variable parameters that can be used to alter the characteristics of the model. In this investigation parameter values of $F_c = 38$ and $\sigma = 2133.4$ were determined to give the best approximation of the experimental results. The comparison of numerical results to experimental results is shown in Figure 14.

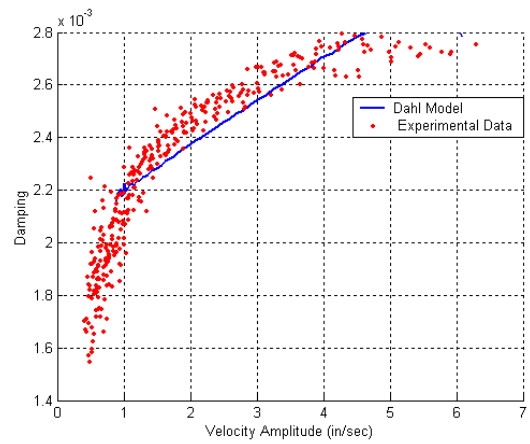

Figure 14: Experimental Results fitted with Dahl model

The LuGre model on the other hand has seven parameters that can be altered and, therefore allows for a more accurate representation of the data. A similar analysis was performed and a damping versus velocity plot illustrating the experimental data and the finite element approximation was created and can be seen in Figure 15. The parameters that were used to create this mathematical model were: $v_d = .95$, $v_0 = 1$, $\sigma_0 = 2133.4$, $\sigma_1 = -.4573$, $\alpha_0 = 10000$, $\alpha_1 = \alpha_0$, and $\alpha_2 = .3731$.

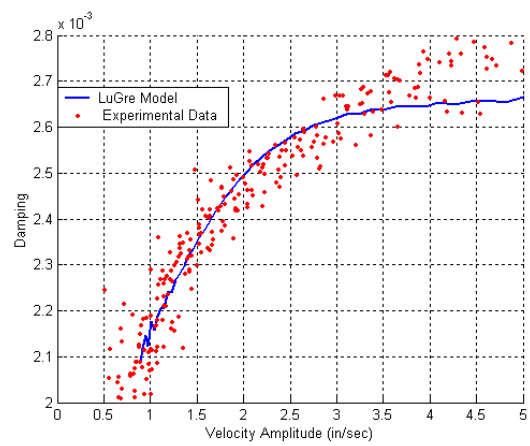

Figure 15: Experimental Results fitted with LuGre model

These results show that the LuGre model more accurately approximates the friction at the bearing surfaces in the lap joints. Despite the fact that the LuGre model more accurately reflects damping in the beam at low velocities, the model diverges from the experimental results at large velocities. Therefore the model does not precisely represent the

experimental results at all amplitudes. Further analysis is needed to develop a more accurate model.

CONCLUSIONS

A combined experimental and analytical investigation was conducted to study (1) the effect of stress distribution in bolted lap joints on energy dissipation, and (2) the plausibility of standard friction models to describe the experimental phenomena.

The experiments conducted in this study confirm and permit a degree of quantification of the two hypotheses regarding lap joint behavior made in the introduction. First, it was shown that the equivalent linear damping is a function of the velocity amplitude for low-level motion. Constant damping force and increased motion at higher response amplitudes correspond to increased damping and energy dissipation. Second, it was shown that the equivalent linear damping in a lap joint is a function of the bearing area over which micro-slip can potentially occur. Because all configurations had the same bolt torque, the larger the bearing areas within the lap joint correspond to lower normal stresses, greater potential for micro-slip, and therefore more micro-slip.

In order to further the understanding of energy dissipation in lap joints, the authors recommend performing tests with more bearing area variations, clamping load variations, alternative geometries of the joint, different materials, and variable washers on the outside of the joint.

ACKNOWLEDGEMENTS

This research project was performed at Los Alamos National Laboratory as part of the Second Annual Los Alamos Dynamic Summer School. Funding for the Los Alamos Dynamics Summer School was provided by the Engineering Science and Applications Division at the Los Alamos National Laboratory and the Dept. of Energy's Education Programs Office. The following companies provided data acquisition hardware and various software packages that were necessary to complete the student projects: Dactron, Inc. (data acquisition hardware), Vibrant Technologies (experimental modal analysis software), The Mathworks, Inc. (numerical analysis software), and ANSYS, Inc. (finite element software).

REFERENCES

Canudas de Wit C., Olsson H., Åström K. J. and Lischinsky P. (1995), "A New Model for Control of Systems with Friction," IEEE Transactions on Automatic Control Vol. 40. No 3.

Dahl P. R. (1976), "Solid Friction Damping of Mechanical Vibrations" AIAA Journal Vol. 14. No 12.

Gaul L., Nitsche R. (2001) "The Role of Friction in Mechanical Joints," Applied Mechanics Reviews, Vol. 54, No 2, pp 93-106.

Haessing D. A., Jr., Friedland B. (1991), "On the Modeling and Simulation of Friction," Journal of Dynamics Systems, Measurements, and Control.

Moloney C. W, Peairs D. M., Roldan E. R., (2000), "Characterization of Damping in Bolted Lap Joints" IMAC-XIX Modal Analysis Conference

Olsson H., Åström K. J., Canudas de Wit C., Gäfvert M., and Lischinsky P. (1998), "Friction Models and Friction Compensation." European Journal on Control.

Thomson W. T. (1988), "Theory of Vibration With Applications". Prentice Hall, Englewood Cliffs: